Journal of the Korean Nuclear Society
Volume 33, Number 4, pp.286~300, August, 2002

Development of Sodium Voiding Model for the KALIMER Analysis

Won-Pyo Chang and Dohee Hahn
Korea Atomic Energy Research Institute
150 Dukjin-dong, Yuseung-gu, Daejon 305-353, Korea
wpchang@kaeri.re.kr

(Received August 29, 2001)

Abstract

An algorithm for the sodium boiling model has been developed for calculation of the void reactivity feedback as well as the fuel and cladding temperatures in the KALIMER core after onset of sodium boiling. Modeling of sodium boiling in liquid metal reactors using sodium as a coolant is necessary because of phenomenon difference comparing with that observed generally in light water reactor systems. The applied model to the algorithm is the multiple-bubble slug ejection model. It allows a finite number of bubbles in a channel at any time. Voiding is assumed to result from formation of bubbles that fill the whole cross section of the coolant channel except for the liquid film left on the cladding surface. The vapor pressure, currently, is assumed to be uniform within a bubble. The present study is focused on not only demonstration of the vapor bubble behavior predicted by the developed model, but also confirmation of a qualitative acceptance for the model. As a result, the model can represent important phenomena in the sodium boiling, but it is found that further effort is also needed for its completition.

Key Words : sodium boiling, KALIMER, SSC-K, HCDA, reactivity feedback

1. Introduction

The Korea Atomic Energy Research Institute (KAERI) has been developing the conceptual design of KALIMER (**K**orea **A**dvanced **LI**quid **ME**tal **R**eactor) [1], which is a sodium cooled, 150 MWe, pool-type reactor. The primary heat transport system (PHTS) of KALIMER is submerged in the big sodium pool, which provides the large thermal inertia of the system. KALIMER, with a metallic fueled core, is designed in such a way that intrinsic negative reactivity feedback effect is expected during the transients including design basis events.

Even though the KALIMER design may not allow boiling at any circumstance under the design basis accidents, sodium boiling is anticipated under HCDA (Hypothetical Core Disruptive Accident) initiating events which are represented by UTOP (Unprotected Transient Over Power), ULOF

(Unprotected Loss Of Flow), ULOHS (Unprotected Loss Of Heat Sink), or sudden flow channel blockage, due to power excursion caused by the reactivity feedback. For a realistic assessment of the HCDA consequence, it is also important to predict the core void in order to estimate the core reactivity feedback.[2] The slug and annular flow regimes tend to prevail for liquid-metal boiling near atmospheric pressure primarily due to high surface tension and low Prandtl number, while the bubbly flow is typical under high pressure in light water reactors.[3,4,5] In this regard, the sodium boiling in liquid metal reactors should be modeled independently because of the phenomenon difference between two reactor systems. Unfortunately, SSC-K [6] which is used as the main code for the KALIMER safety analysis is not capable of analyzing the sodium boiling so far. To this end, the algorithm for the sodium boiling model has been developed in order to extend the applicable range of SSC-K.

There are a few codes capable of analyzing the HCDA initiating events for liquid metal reactors. SAS series [5] and FRAX [7,8,9] codes may be representatives on this area. They basically use the multi-bubble slug ejection model, which represents boiling coolant with multi liquid slugs divided by bubbles.

2. Theory for Sodium Boiling Model (SOBOIL)

Sodium boiling model in SOBOIL is basically multi-bubble slug ejection model similar to that used in SAS2A.[5] Since the interfaces between the liquid slugs and a vapor bubble are moving, a model which uses only fixed nodes is not be likely to be good enough. Voiding is assumed to result from formation of bubbles that fill the whole cross section of the coolant channel except for liquid film left on the cladding or structure. A finite

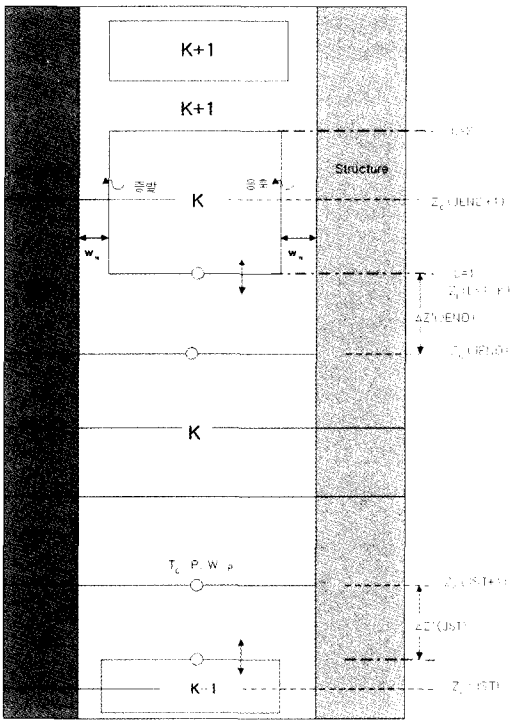

Fig. 1. Nodalizations for 'SOBOIL' Model

number of vapor bubbles, separated by liquid slugs, are allowed in the channel at any time. The liquid film around the vapor is assumed to be static currently, its motion, however, will be improved later.

2.1. Liquid Slug Flow Rates

The description of the momentum conservation equation for the liquid flow is similar to that used in SAS2A, except expressing it with flow rate instead of mass flux in order to take account of the flow area variation for a node in the numerical computation. The integral liquid momentum equation is given by

$$\frac{1}{A_c}\frac{\partial W}{\partial t}+\frac{\partial P}{\partial z}+\frac{1}{A_c}\frac{\partial (Wv)}{\partial z}=-\left(\frac{\partial P}{\partial z}\right)_{fr}-\left(\frac{\partial P}{\partial z}\right)_{K}-\rho_c g \quad (1)$$

The momentum equation is applied to each slug

which is represented in the Fig. 1, individually, and is integrated over the length of each slug rather than over the length of the channel. One can obtain

$$I_1 \frac{\partial W}{\partial t} + P_t - P_b + W^2 I_2 + A_{fr} W|W|^{1+b_{fr}} I_3 + W|W| I_4 + g I_5 = 0 \quad (2)$$

where,

$$I_1 = \int \frac{dz}{A_c} = \sum_{JC=JST}^{JEND} X_{I1}(JC), \quad X_{I1}(JC) = \frac{\Delta z(JC)}{A_c(JC)} \quad (3)$$

$$I_2 = \sum_{JC=JST}^{JEND} X_{I2}(JC), \quad X_{I2}(JC) = \frac{1}{A_c(JC)^2}\left[\frac{1}{\rho_c(JC+1)} - \frac{1}{\rho_c(JC)}\right] \quad (4)$$

$$I_3 = \int \frac{1}{2\rho_c A_c^2 D_h}\left[\frac{D_h}{\mu A_c}\right]^{b_{fr}} dz = \sum_{JC=JST}^{JEND} X_{I3}(JC)$$

$$X_{I3}(JC) = \frac{\Delta z(JC)}{\left[\rho_c(JC) + \rho_c(JC+1)\right] A_c(JC)^2 D_h(JC)}\left[\frac{D_h(JC)}{\bar{\mu}(JC) A_c(JC)}\right]^{b_{fr}}$$

$$I_4 = \sum_{JC=JST}^{JEND} K_{OR}(JC) \quad (6)$$

$$I_5 = \int \rho_c \, dz = \sum_{JC=JST}^{JEND} X_{I5}(JC), \quad (7)$$

$$X_{I5}(JC) = 0.5\left[\rho_c(JC) + \rho_c(JC+1)\right] \Delta z(JC)$$

The integer variable JST is the number of the mesh segment in which the bottom of the liquid slug is located, while JEND is the number of the segment in which the top is contained. Since the integration is over only the liquid portions of these segments, the axial length terms Δz (JC) in the expressions for X_{I1}, X_{I3}, and X_{I5} must be altered as follows :

$$\text{If } K > 1 \; \Delta z'(JST) = z_c(JST+1) - z_i(L=2,\ t,\ K-1)$$

$$\text{If } K = 1, \quad \Delta z'(JST) = \Delta z(JST)$$

$$\text{If } K < K_{vn}, \; \Delta z'(JEND) = z_i(L=1,\ t,\ K) - z_c(JEND)$$

$$\text{If } K > K_{vn}, \quad \Delta z'(JEND) = \Delta z(JEND)$$

where K is the vapor number with the numbering going from 1 for the lawest bubble in teh channel to k_{vn} for the highest, and $z_i(L,t,K)$ denotes the location of the interface between the liquid and the vapor K, L=1 for the lower interface of the bubble K, and L=2 for the upper interface.

In the special case of a small liquid slug entirely contained within one mesh segment, JST = JEND. Then,

$$\Delta z'(JST) = z_i(L=1,\ t,\ K) - z_i(L=2,\ t,\ K-1) \quad (8)$$

and there is only one term in each of the summations for I1 through I5 . The final numerical equation is then,

$$I_1|_{t+\Delta t}\frac{\Delta W}{\Delta t} + \left(P_t|_{t+\Delta t} - P_b|_{t+\Delta t}\right) + I_2|_{t+\Delta t}\left(W_1^2 + 2\theta_2 W_1 \Delta W\right) + A_{fr} I_3|_{t+\Delta t}\left[W_1|W_1|^{1+b_{fr}} + \left(2+b_{fr}\right)|W_1|^{1+b_{fr}}\Delta W\right] + I_4|_{t+\Delta t}\left(W_1|W_1| + 2\theta_2|W_1|\Delta W\right) + I_5|_{t+\Delta t} g = 0 \quad (9)$$

All I' s in Eq. (9) except I_5 are assumed to be constant over the time step because the liquid interface density is considered to make a very small effect and can be neglected. Since the interface location changes with time,

$$I_5(t) = \int_{z_{JST}(t)}^{z_{JEND}(t)} \rho_\ell(z)\, dz \quad (10)$$

and at t + Δt,

$$I_5(t+\Delta t) = \int_{z_{JST}(t+\Delta t)}^{z_{JEND}(t+\Delta t)} \rho_\ell(z) dz \quad (11)$$

Taking the difference for these two variables

$$I_5(t+\Delta t) - I_5(t) = \int_{z_{JEND}(t)}^{z_{JEND}(t+\Delta t)} \rho_\ell(z)\, dt - \int_{z_{JST}(t)}^{z_{JST}(t+\Delta t)} \rho_\ell(z) dz \quad (12)$$

because these two integrals, Eq. (10) and Eq. (11) are identical except in segment JST and

JEND, where the bubble interface positions are changing with time. The interface position z_i can be written as a linear function of the interface velocity, v_i so that

$$dz = v_i \, dt \tag{13}$$

Therefore, I_5 (t + Δt) is

$$I_5(t+\Delta t) = I_5(t) + \rho_{ti}(JEND) \int_t^{t+\Delta t} v_i(L=1, t', K)\, dt' - \rho_{ti}(JST) \int_t^{t+\Delta t} v_i(L=2, t', K-1)\, dt' \tag{14}$$

If the velocity is assumed to vary linearly over the time step, the time integrals in (14) becomes

$$I_5(t+\Delta t) = I_5(t) + \rho_{ti}(JEND) v_i(L=1, t, k)\left(1+\frac{\Delta W}{2W_1}\right)\Delta t - \rho_{ti}(JST)\, v_i(L=2, t, k-1)\left(1+\frac{\Delta W}{2W_1}\right)\Delta t \tag{15}$$

Similarly, I_1 (t + Δt) and I_3 (t + Δt) also can be expressed in the same way.

Thus, change in flow rate for a liquid slug in Eq. (9) is related to change in vapor pressure in the bubble above and below the liquid slug, or to change in the inlet and outlet coolant pressures.

2.2. Liquid Temperature

Since the interface moves along the axis, both Eulerian and Lagrangian schemes are used for computing transient temperatures in the liquid coolant. The Eulerian scheme is usually applied before incipient boiling, while the Lagrangian scheme is used for all liquid slugs other than the inlet liquid slug after boiling. However, Lagrangian scheme is also used for the inlet liquid slug with a low flow rate (~ 10 % of the initial flow rate).

For the Eulerian scheme, the basic energy equation in a liquid slug is given by

$$\rho_t c_t \frac{\partial T_c}{\partial t} + G c_t \frac{\partial T_c}{\partial z} = \varphi(z,t) + Q_c(z,t) \tag{16}$$

Eq. (16) is numerically discritized with semi-implicit method in time and space, e.g.

$$\frac{dT_c}{dt} = \frac{1}{2}\left[\frac{T_c(z+\Delta z, t+\Delta t) - T_c(z+\Delta z, t)}{\Delta t} + \frac{T_c(z, t+\Delta t) - T_c(z,t)}{\Delta t}\right] \tag{17}$$

For the Lagrangian scheme, it is used to calculate the liquid coolant temperatures both at the fixed axial mesh points and at the moving points near the liquid-vapor interfaces. The Lagrangian total time derivative, dT_c/dt, as seen by an observer moving with the coolant velocity, is used and axial heat conduction through the interfaces is ignored in the calculation. This derivative is approximated by

$$\frac{dT_c}{dt} = \frac{T_c(z, t+\Delta t) - T_c(z-\Delta z, t)}{\Delta t} \tag{18}$$

where

$$\Delta z = \frac{[G(t+\Delta t) + G(t)]\Delta t}{2\bar{\rho}(z)}, \quad \bar{\rho}(z) = \rho(T_c(z, t+\Delta t/2)) \tag{19}$$

The basic equation for the interface liquid temperature, $T_{ci}(t+\Delta t)$, by the Lagrangian formulation is numerically given by

$$\bar{\rho}\bar{c}\frac{T_{ci}(t+\Delta t) - T_{ci}(t)}{\Delta t} = \frac{1}{2}[\varphi(t+\Delta t) + \varphi(t)] + \bar{Q}_c \tag{20}$$

where φ are now defined as

$$\varphi(t+\Delta t) = h_{eci}(t+\Delta t)[T_{ei}(t+\Delta t) - T_{ci}(t+\Delta t)] \tag{21}$$

$$\varphi(t) = h_{eci}(t)[T_{ei}(t) - T_{ci}(t)] \tag{22}$$

The subscript i refers to values at the interface and T_{ei}, T_{ci}, and h_{eci} indicate wall temperature, coolant temperature, and heat transfer coefficient between wall and coolant, respectively. Since the cladding or structure temperatures are only calculated at the fixed axial mesh points, T_{ei} is obtained by linear interpolation from the mesh-

point values. The values of $\bar{\rho}$ and $\bar{c}$ are obtained using the extrapolated interface temperature at $t+\Delta t/2$. Since direct heating of the coolant is normally a small effect, and ignored in the present model. (i.e. $\bar{Q}_c = 0$).

The Lagrangian calculation for the coolant temperatures at fixed axial mesh points is similar to Eq. (20) and the resulting equation is given by

$$T_c(z,t+\Delta t) = \frac{T_c(z-\Delta z,t)(1-d_1\bar{h}_1) + d_1\varphi_1}{1 + d_1\bar{h}_2} \quad (23)$$

where Δz is given by Eq. (19), and the temperatures $T_c(z - \Delta z, t)$ and $T_e(z - \Delta z, t)$ are obtained by linear interpolation from the values at the fixed mesh points.

2.3. Heat Conduction Equation

A one-dimensional heat conduction equation is set up in order to calculate the temperature distribution within the fuel or structure with given boundary conditions in a cylindrical coordinate. The numerical method is applied to solving the equation because analytical method is not suitable for complex geometry and physical properties of the solid with non-uniform heat generation rate. This model is developed primarily with a semi-implicit method. The maximum of 50 nodes in the radial direction are currently allowed for solving the equations.

2.3.1. Governing Equation

A general form of the conduction equation is rewritten for one dimensional problem as

$$\rho c\frac{\partial T}{\partial t} = k\frac{d^2T}{dx^2} + q''' \quad (24)$$

2.3.2. Inner Nodes

Integrating Eq. (24) over the node volumes and

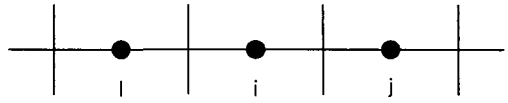

Fig. 2. Control Volume for Heat Conduction Equation

differentiate it from node j to node l, the resulting equation is given through some arrangement by :

$$\rho_i c_i V_i\frac{\partial T_i}{\partial t} + \left[-\frac{k_{ij}A_{ij}}{d_{ij}}T_j - \frac{k_{il}A_{il}}{d_{il}}T_l + \left(\frac{k_{ij}A_{ij}}{d_{ij}} + \frac{k_{il}A_{il}}{d_{il}}\right)T_i\right] = q_i''' V_i \quad (25)$$

The Eq. (25) is, then, defined in the following way to express in the matrix form

$$\rho_i c_i V_i = cmat(i) \quad (26)$$

$$-\frac{k_{ij}A_{ij}}{d_{ij}}T_j = smat3(i) \quad (27)$$

$$-\frac{k_{il}A_{il}}{d_{il}}T_l = smat1(i) \quad (28)$$

$$\frac{k_{ij}A_{ij}}{d_{ij}} + \frac{k_{il}A_{il}}{d_{il}} = smat2(i) \quad (29)$$

$$q_i''' = rmat(i) \quad (30)$$

$$cmat(i)\frac{dT_i}{dt} + [smat3(i)T_j + smat1(i)T_l + smat2(i)T_i] = rmat(i) \quad (31)$$

where, dT/d_t can be expressed as $T_i^{n+1} - T_i^n)/\Delta t$, and Crank-Nicolson scheme which defines T with the average of the previous and advanced time step values, is applied to Eq. (31). Then, Eq. (31) can be rewritten as

$$cmat(i)\frac{T_i^{n+1} - T_i^n}{\Delta t} + [smat3(i)(\frac{T_j^{n+1} + T_j^n}{2}) + smat1(i)(\frac{T_l^{n+1} + T_l^n}{2}) + smat2(i)(\frac{T_i^{n+1} + T_i^n}{2})] = rmat(i) \quad (32)$$

The linear equation (32) is finally solved iteratively due to the non-linearity.

2.4. Bubble Formation and Collapse

2.4.1. Basic Assumptions for Vapor Bubble Modeling

The present SOBOIL model has been developed based on the uniform pressure model which is adequate to small bubbles. For small bubbles, the pressures may be assumed to be uniform spatially inside the bubbles, whereas there exists a pressure gradient for a bubble length exceeding the specified minimum size. Thus, a different model must be applied because axial distribution of the pressure cannot be ignored. This model, however, will be considered in the present model.

Vapor is formed if a specified amount of superheat is satisfied at a node in the model. If the specified amount of superheat is exceeded in a node, then time-step size is reduced, and coolant calculations for the channel are repeated for the time step, so as to satisfy the superheat criterion exactly at the end of time step. This model, however, is subjected to the following limitations.

(i) No new vapors will be formed within a minimum distance adjacent to a vapor-liquid interface, and thus, nodes within the distance from the interface are not examined for bubble formation ;

(ii) No more than one bubble will be formed within a time-step

(iii) Vapors are always saturated at given temperatures.

(iv) If vapor temperature change exceeds a specified amount, the time-step is also reduced.

(v) A new vapor generated in a liquid slug divides the liquid slug into two liquid slugs and the initial liquid flow rates for these two liquid slugs are assumed same as that of the liquid slug before the voiding.

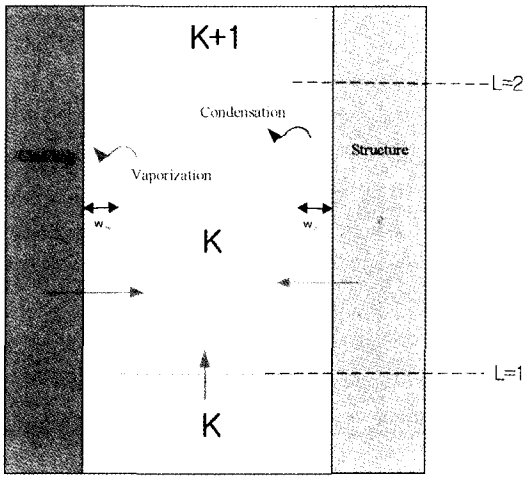

Fig. 3. Unidoem Pressure Vapor Model

Fig. 3 shows the control volume considered in the uniform vapor pressure model. Vapors are assumed to fill the whole cross section of the coolant channel, except for a liquid film left on the cladding or structure. The shrink of the vapor bubble is possible because of condensation in the cooler region. When vapor length and decreasing rate of the size are simultaneously below the minimum values, the vapor disappears. Two liquid slugs are also combined into one if the gap between two vapors is close enough each other.

The bubble growth is determined by coupling the momentum equations for the liquid slugs with energy balance in the vapor bubble, assuming saturation condition and spatially uniform pressure and temperature within a vapor. The rate of formation and condensation of the vapor is determined by the heat flow through the liquid film on the cladding or structure, and through the liquid-vapor interfaces. The primary focus of this model is to obtain the temperatures within the vapor bubbles. Once the temperatures are known, it

can be used to calculate the vapor pressures, since the saturation conditions are assumed. The vapor pressure is the driving force for the motion of the liquid slugs, so finding the vapor pressures in all the bubbles provides the link between conditions in the liquid slugs and conditions in the vapors. Therefore the vapor pressure leads to a complete description of the vapor conditions throughout the channel.

2.5. Energy Transfer Into Uniform Pressure Bubble

The total energy added to vapor bubble K in a time step is

$$Q_t = \int_t^{t+\Delta t} [\, Q_{es}(\tau) + Q_i(\tau) \,]\, d\tau \tag{33}$$

Q_{es} is the heat flow from the heat structure and approximated by

$$Q_{es} = \frac{\Delta t}{2}\left[Q_{es}(k,t) + Q_{es}(k,t+\Delta t) \right] \tag{34}$$

where,

$$Q_{es}(k,t) = P_e \int_{Z_i(L=1,4,K)}^{Z_i(L=2,t,K)} q_e(z,t)\, dz \tag{35}$$

Using the interface position defined in the nomenclature, the integral for the heat flow Q_{es}(K, t+Δt) can be expressed as the sum of three integrals :

$$\begin{aligned} Q_{es}(K,t+\Delta t) = {} & P_e \int_{z_{i0}(k,1)}^{z_{i0}(k,2)} q_e(z,t+\Delta t)\, dz \\ & + P_e \int_{z_{i0}(K,2)}^{z_{i0}(K,2)+\Delta z'(K,2)} q_e(z,t+\Delta t)\, dz \\ & + P_e \int_{z_{i0}(K,1)+\Delta z'(K,1)}^{z_{i0}(K,1)} q_e(z,t+\Delta t)\, dz \end{aligned} \tag{36}$$

where $\Delta z'(K',L)$ denotes the interface position change caused by the vapor pressure changes over a time-step. If the vapor temperature T(K, t + Δt) is linearized to be T(K, t) + ΔT(K), the first integral is a function only of ΔT(K) and known quantities, since the advanced time cladding temperatures are determined by extrapolating from the temperature slopes calculated at the previous time-step and, therefore, are considered known.

2.6. Heat Flow Through Liquid-vapor Interface

Calculation of the interfacial heat transfer between liquid and vapor in the SOBOIL model is directly based on that in SAS2A [2]. In this method, total heat flow through the liquid-vapor interfaces is the sum of the upper interface term and lower interface term

$$Q_i = \Delta t\left(I_{iu} + I_{il} \right) \tag{37}$$

where

$$I_{ix} = k_\ell A_{cx} \left.\frac{\overline{\partial T}_{\ell x}}{\partial \xi}\right|_{\xi=0} \tag{38}$$

with

x = u or l

A_{cx} = Area of coolant channel

T_{lx} = Liquid temperature near interface

ξ = Axial distance from interface

ξ = z - z_i for upper interface

ξ = - (z - z_i) for lower interface

$\frac{\overline{\partial T}_{\ell x}}{\partial \xi}$ = Time average of the spatial derivative for the time step.

An expression for the coolant temperature derivative $\frac{\overline{\partial T}_{\ell x}}{\partial \xi}$ can be derived from the general heat conduction equation;

$$\alpha \frac{\partial^2 T_\ell(\xi, t')}{\partial \xi^2} + \frac{Q(\xi, t')}{\rho_\ell C_\ell} = \frac{\partial T_\ell(\xi, t')}{\partial t'} \tag{39}$$

The boundary conditions for the problem are:

$T_l(\xi = 0, t') = T(t')$, the liquid temperature at the liquid-vapor interface

$T_l(\xi = \infty, t') < \infty$,

The initial condition is:

$T_l(\xi, t' = 0)$ *known*

The heat conduction equation, Eq. (39), together with the initial and boundary conditions, can be solved for T_l using the Laplace transform method.

2.7. Change in Vapor Energy

The heat flow into the vapor control volume is used both to produce a new vapor and to raise the temperature of already existing vapor. During a time interval Δt, the vapor temperature goes from T to T+ΔT, the pressure goes from P_V+ΔP, the density goes from $\rho_V + \Delta\rho_V$, the bubble volume goes from V_v to $V_v + \Delta V$, and the vapor energy changes by ΔE. The ΔP and ΔV are related to ΔT by the requirement that saturation conditions prevail in the vapor.

Two processes contribute to energy change ΔE. One is the heating of the quantity of vapor present at the beginning of the time step from temperature T to temperature T+ΔT. The other is the vaporization of some of the liquid film to an additional vapor, giving a total vapor mass of $(\rho_v + \Delta\rho_v)(V_v+\Delta V)$ at the end of the time step. However, it is not straightforward to formulate an expression for the energy change by directly considering the heating of the vapor (because of the volume and density changes which take place during the heating) and the vaporization of some liquid film (because the amount of film vaporized is unknown). Therefore, a thermodynamically equivalent path is considered instead of straightforward expression of the energy change. This path can be described in the following three steps:

Step 1: condense the vapor in the bubble at time t to liquid at constant pressure and temperature

Step 2 : heat the liquid from step 1 to T+ΔT:

Step 3 : vaporize the liquid from step 2 plus enough liquid from the film to fill the volume $V_v+\Delta V$:

2.8. Energy Balance

The energy balance between the energy transferred to the control volume and the energy change within the volume, determines change of the vapor energy. The energy transferred to the volume, E_t, is sum of energy flow from the cladding or structure, Q_{es}, and the energy flow through the liquid-vapor interfaces, Q_i, in Eq. (33). can further be expressed as a linear function of the change in the vapor temperature, ΔT.[5] When E_t is combined with together, the resulting equation is a linear equation in terms of the changes in the vapor temperatures of bubbles K-1, K, and K+1, which may be arranged as:

$$C_1(K)\Delta T(K-1)+C_2(K)\Delta T(K)+C_3(K)\Delta T(K+1) = C_4(K) \quad (40)$$

In general, if a series of N bubbles of uniform vapor pressure extends from the bottom to top of the channel, then temperature changes in the N bubbles are calculated by solving a set of linear equations written in terms of N unknowns. Once the vapor temperatures are known, the saturation conditions are used to obtain the vapor pressures.

3. Overview of Basic Calculation Scheme

The present model is summerized as the following steps in the calculation:

(1) It first reads input variables that users must supply for the calculation and then determines

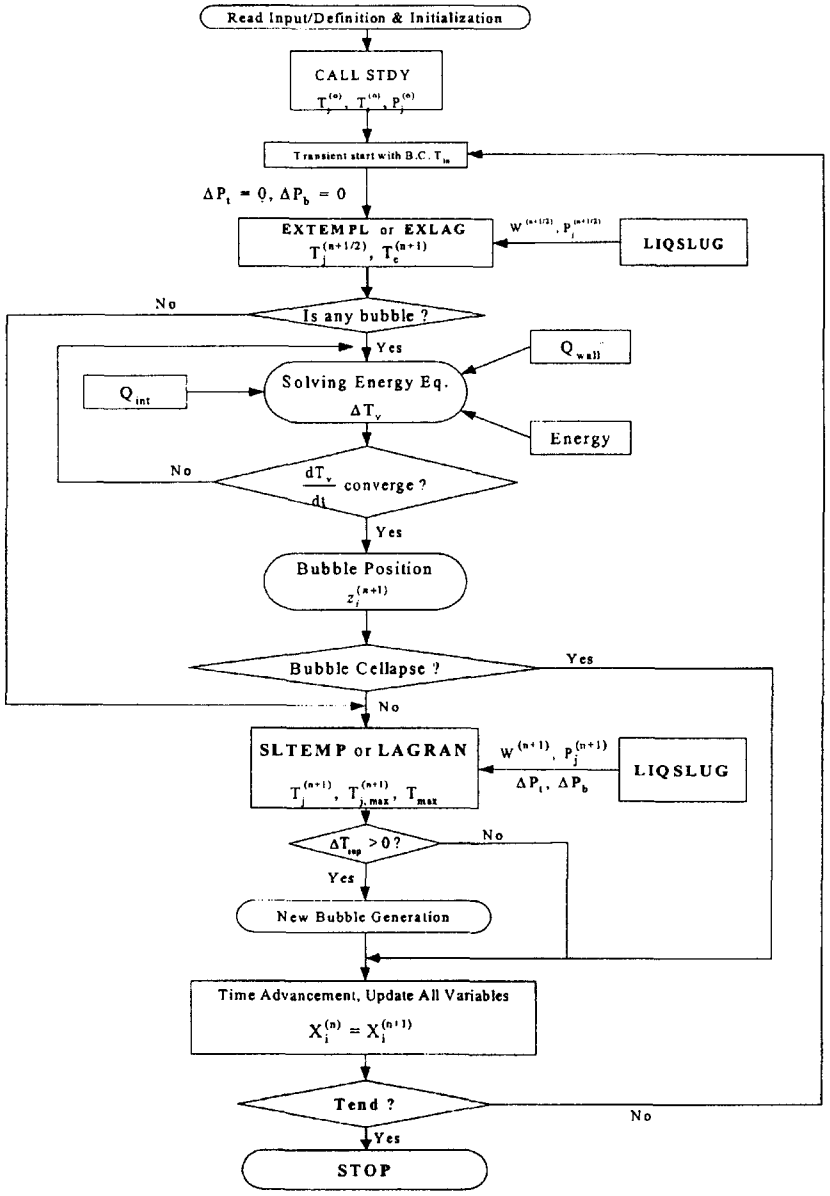

Fig. 4. Flow Diagram of SOBOIL Model

the steady state conditions for temperature and pressure distributions in the liquid slug, and wall temperatures using the input data. It also defines various initial conditions for the transient calculation.

(2) Calculate the preliminary flow rates and temperature distributions in the liquid slugs together with wall temperatures for new time step

- Calculations of the temperature distribution and flow rate in each liquid slug separated by bubbles with neglecting the effect of changes

in the vapor bubble pressures over the time step

(3) Calculate the advanced vapor temperatures if there were vapors in the channel. An iterative process is necessary in this calculation, because the advanced vapor temperatures are used for the calculations of both the interfacial and temperature.

(4) Finally, calculation of the advanced time pressures, temperatures, and mass flow rates using physical properties and wall temperatures evaluated at the pre-estimated temperatures and flow rates in the liquid slug.

In all iteration processes, the time step is reduced when the number of iteration exceeds some specified number. When the preliminary wall temperatures and liquid flow rate change are radical, and vapor temperature change is large, the time-step is reduced into a half of the former value. Fig. 4 illustrates the flow chart for this scheme.

4. Results and Discussions

The KALIMER design parameters for the active core channel are used. The initial values for SOBOIL are obtained from the steady state results of the ULOHS analysis using SSC-K. The main parameters used in order to verify the developed SOBOIL model are summarized in Table 1.

Fig. 5 and 6 are the profiles of the steady state temperatures and pressure in the channel, respectively, while Fig. 7 illustrates the radial temperature distribution inside the fuel pin. The pressure decreases linearly along the channel as expected with a constant flow rate. The coolant and cladding temperatures also exhibit the expected profiles. The fuel centerline temperature at outlet is lower than that of the down node in Fig. 7. It attributes to lower heat generation rate at the end than at the down node in the fuel.

For the transient, the core inlet coolant temperature is assumed to increase 50 °K/sec while the inlet coolant pressure keeps the constant value as given in Table 1, taking account of a condition during the ULOHS accident. Because a newly generating vapor gets the saturation pressure corresponding to the specified superheated temperature of the liquid coolant from the vapor generation criteria, the vapor pressure is higher than the liquid pressure at that point by amount of the superheat. Consequently, pressure jump occurs when a new vapor is generated in the present model. Fig. 8 is result of pressure change of the first vapor with time. The vapor initially grows due to the pressure jump as well as the heat transfer from the liquid near the interface into the vapor. These two effects

Table 1 Parameters for SOBOIL Verification

Parameters	Values used in SOBOIL	Parameters	Values used in SOBOIL
Active Core Height (m)	1.2	Fuel Pallet Radius (m)	2.73 x 10-3
Flow Area (m^2)	2.87×10^{-5}	Cladding Inner Radius (m)	3.15 x 10-3
Hydraulic Diameter (m)	2.87×10^{-5}	Cladding Outer Radius (m)	3.70 x 105
Perimeter (m)	0.0074	Time-Step (ms)	5.0
Initial Liquid Flow (kg/s)	0.14686	No. of Axial Nodes	20
Inlet Coolant Temp. (°K)	1150.70	No. of Radial Nodes	6
Inlet Coolant Pressure (Pa)	4.30×10^{5}	in the Fuel Pallet	
Outlet Coolant Pressure (Pa)	4.0×10^{5}	No. of Radial Nodes in the cladding	3

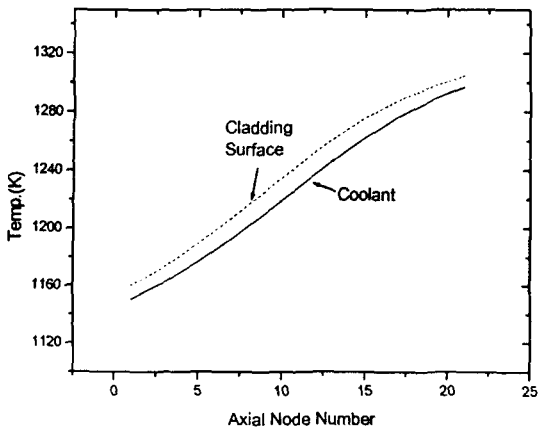

Fig. 5. Axial Temp. Profiles in the Fuel Fin

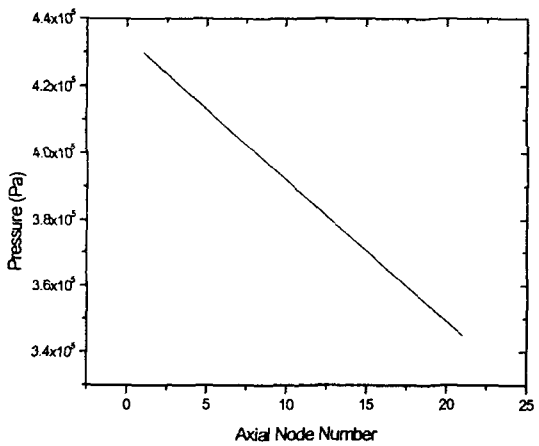

Fig. 6. Steady-State Pressure Profile

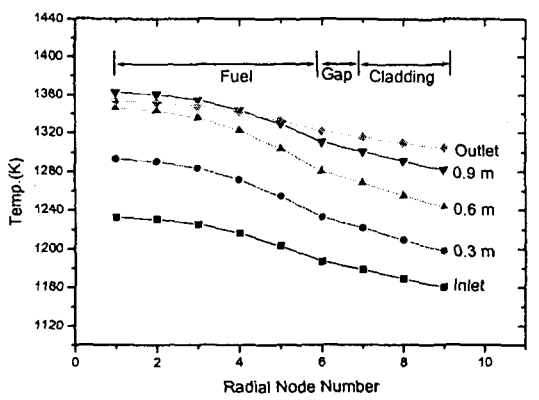

Fig. 7. Radial Temp. Profiles in the Fuel Pin

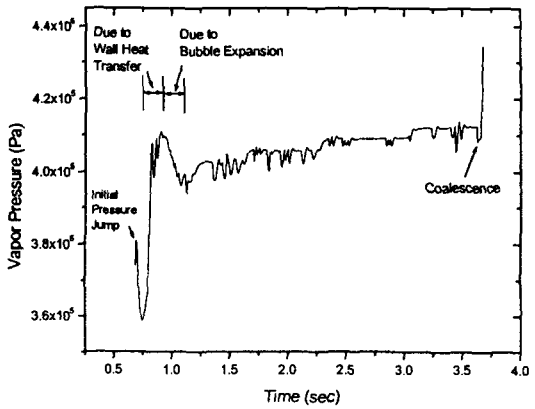

Fig. 8. Vapor Pressure Change with Time

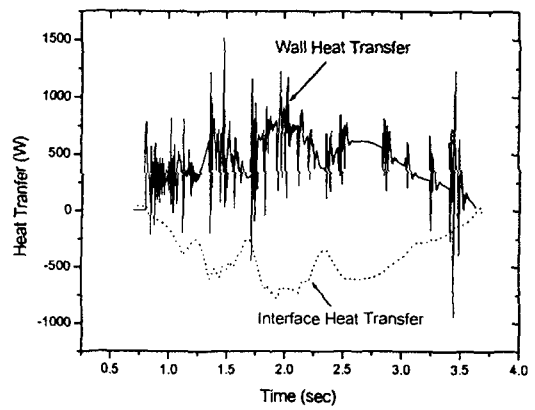

Fig. 9. Wall and Interface Heat Transfers

accelerate the vapor growth in the early period. After the pressure jump, the vapor pressure decreases for a short period, mainly due to the initial volume expansion. As the vapor gets larger and it exceeds a certain size, amount of the heat transfer from the wall (fuel) begins larger than the heat transfer from the vapor to the liquid slug at the interface as seen in Fig. 9. The fast increase of the vapor pressure also causes the lower interface of the vapor to move downward rapidly. The sudden increase of the vapor pressure near 0.75 sec in Fig. 8 gives rise to reduction of the flow rate for the liquid slug below the vapor, because the pressure difference for the upper and lower

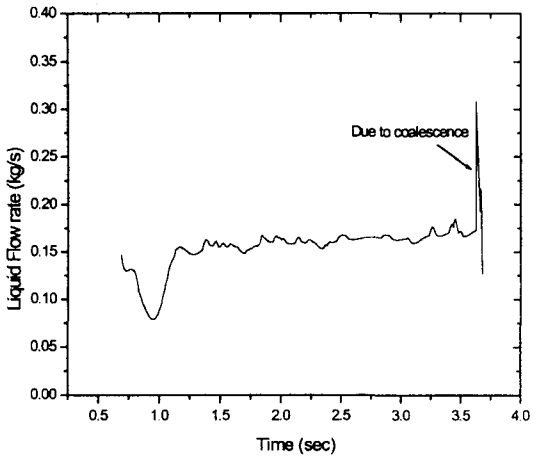

Fig. 10. Liquid Slug Flow Rate with Time

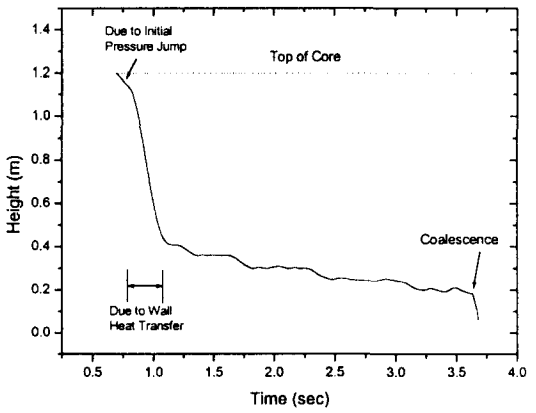

Fig. 11. Development of the Vapor Interface

boundaries for the liquid slug gets smaller. The flow behavior is well represented in Fig. 10. Accordingly, the wall heat transfer as well as reduction of the flow rate for the liquid slug below the vapor mostly contributes to the rapid development of the lower interface of the vapor around 1.0 sec shown in Fig. 11. The sudden expansion of the vapor region also leads to slowing down the rate of the vapor pressure increase. The flow rate for the liquid slug below the vapor also goes up as the vapor pressure gets lower. (Fig. 10) Finally, the amount of heat

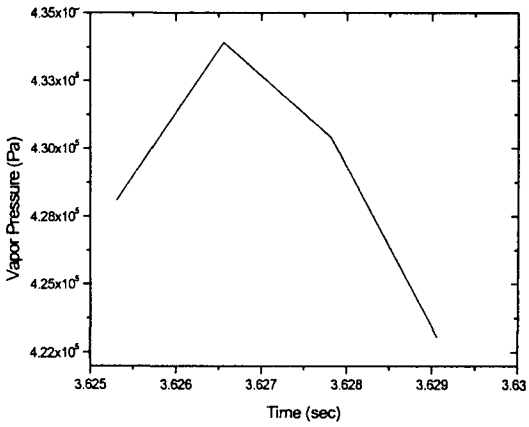

Fig. 12. Pressure Change for the Second Vapor

transfer from the wall and that from the vapor to the liquid near the interfaces are almost balanced as the vapor gets larger. The vapor behavior, thereafter, shows relatively a very slow trend. Such the slow response of the vapor leads to smooth change for the lower interface of the vapor until another vapor is formed below the vapor at about 3.625 sec.

The bubble behavior is more clearly demonstrated through the behavior of the second vapor represented from Fig. 12 to 15. The initial increase of the pressure reduces the liquid flow rate similar to the first vapor and the upper interface moves upward much faster than the lower interface. It is obviously demonstrated from Fig. 15 that the wall heat transfer influences dominantly to the vapor enlargement. The liquid slug located above the new vapor gets shorter. In the SOBOIL model, when a gap size between two vapors reduces below a specified length, two vapors are to coalesce and merge into one. Another dramatic expansion of the lower interface around 3.63 sec in Fig. 11 corresponds to the consequence of this phenomenon. The second vapor exists only for ~ 4 ms. Since the pressure of the vapor emerging due to the coalescence is assumed as an average value of the two pressures

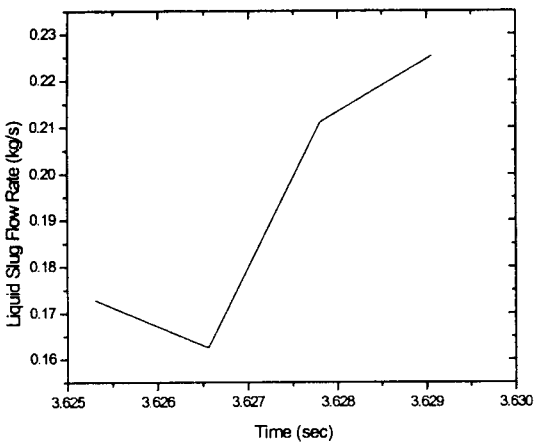

Fig. 13. Liquid Slug Flow Rate for the Lowest Liquid Slug

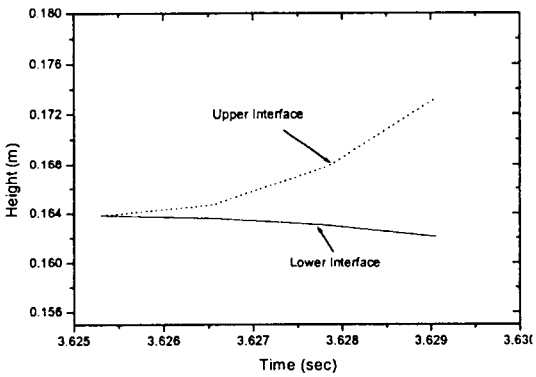

Fig. 14. Interface Developments for The Second Vapor

at the present time, the vapor pressure shows a peak shape in Fig. 8. Similarly, the liquid flow rate also shows a peak behavior around this time because it is replaced with that for the liquid slug below the disappearing vapor.

As a result, the steady state calculations are considered to be reasonable. As the power generation goes up, the slope of the coolant temperature along the flow direction also increases. It smoothens out near the top of the channel because the power generation decreases

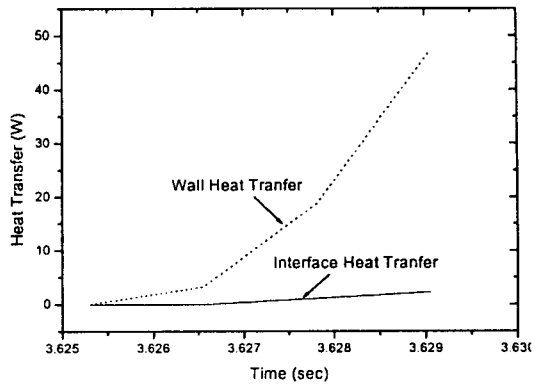

Fig. 15. Wall and Interface Heat Transfers for the Second Vapor

there. Generally, the process for the vapor formation and initial growth agrees with the physical behaviors qualitatively those assumed in the present model. The initial vapor growth is similar to a result presented in the CABRI analysis using FRAX-5 and SAS4A, where sudden downward enlargement of vapor region was predicted within a short time, ~ ms. [9] However, the severe fluctuation shown on the wall heat transfer is not clearly understood at this time, because the vapor size is likely to exceed the applicable range of the present model. The homogenous model that assumes saturation condition with uniform pressure within a vapor is known to be not valid when the vapor size does exceed a certain value. [5] Thus, the vapor temperature as well as pressure can not be assumed same within such a large vapor. Another point is that some user specified parameters in the model, e.g. the conditions for vapor formation, liquid gap distance for the vapor coalescence, time-step reduction criteria, etc. are not physically justified at this time.

5. Conclusions

Most of physical phenomena predicted by the

present model seem to be reasonable qualitatively, at least so that a basis for the complete modeling of the sodium boiling model may be established. It is confirmed that the vapor is obviously the driving force for motion of the liquid slug. The vapor pressure is quite sensitive to its volume change, and the balance between the wall and interface heat transfers is also found out to be important to the vapor volume change. It is noted that if a more general model were applied to the present problem, flow reversal might be possible. Therefore, a more sophisticated verification for validity of the model should be followed. An additional model which can describe the annular flow regime within the large vapor, is also to be developed for the complete analysis of the sodium boiling.

It is learned from this analysis that the sodium voiding develops so rapidly that a large reactivity insertion may be possible in the core within a short time, and thus it may threaten the fuel integrity during the accidents under which the sodium boiling is anticipated. Therefore, it is very important to predict the phenomena accurately in order to understand the detailed fuel behavior caused by the reactivity feedback in the KALIMER core. The effort will be continued to improve the problems identified, and the model finally will be coupled to the SSC-K code to extend its capability.

Acknowledgement

This work was performed under the Long-term Nuclear R & D Programs sponsored by the Korea Ministry of Science and Technology.

Nomenclatures

A_{ij} conduction heat transfer area between node i and j, (Eq.(25))

d_{ij} distance between node i and j, (Eq.(25))

d_1 $\frac{\Delta t}{2\,\bar{\rho}\,\bar{c}}$, definition in Eq. (23)

G liquid mass flow rate (kg/s-m^2)

$\bar{h}_1$ cladding-to-coolant interface heat transfer coefficient at t, (Eq. (23))

$\bar{h}_2$ cladding-to-coolant interface heat transfer coefficient at $t+\Delta t$, $h_{eci}(t+\Delta t)$ (Eq. (23))

k_{ij} thermal conductivity between node i and j, (Eq.(25))

P_b pressure at the bottom of the slug (Eq. (2))

P_t pressure at the top of the slug (Eq. (2))

P_e perimeter of cladding, (Eq. (36))

q_e cladding-to-vapor heat flux (Eq. (36))

$Q_c(z, t)$ volume source due to direct heating by neutrons and gamma rays (w/m^3) (Eq. (16))

Q heat input per unit volume in the liquid, (Eq.(39))

r_e nominal radius of cladding

t' time since the vapor bubble started to form, (Eq.(39))

V_i volume of the conduction control volume i (Eq.(25))

Δ_w changes of liquid slug flow rates over a time-step

$\Delta w_0(K')$ changes of liquid slug flow rates for the upper and lower liquid slug of a vapor bubble over a time-step

$z_{i0}(K, L)$ liquid-vapor interface position without changing bubble pressures, $z_i(L, t, K) + \Delta z_0(K, L)$, (Eq. (36))

$\Delta z_0(K,L)$ liquid-vapor interface position change during Δt without changing bubble pressures,

$$v_i(L,t,K)\Delta z + \frac{1}{2} + \frac{\Delta w_0(K')\Delta t}{2(\rho_t A_c)_{K'L}},$$ (Eq. (36))

$\Delta z_0(K,L)$ liquid-vapor interface, L = 1 for lower interface, L = 2 for upper interface

Greek Symbols

α the thermal diffusivity of liquid sodium, $k_l/\rho l C_l$, (Eq. (39))

c_l liquid specific heat

$\bar{c}$ time average liquid specific heat

φ_1 $h_{ec}(z,t+\Delta_t)\mathrm{Te}\ (z,t+\Delta t) + h_{ec}(z,t)T_e(z-\Delta z,t)$ definition in Eq. (23)

$\varphi(z,t)$ wall heat flow per unit coolant volume (w/m^3) (Eq.(16))

k_l liquid thermal conductivity

ρ_l liquid density

$\bar{\rho}$ time average liquid density

ρ_i, c_i density, and specific heat of the conduction control volume i, respectively

References

1. Dohee, Hahn, et al., "Safety Performance of Preliminary KALIMER Conceptual Design," 7th Int. Conf. on Nuclear Engineering (ICONE-7), Kyoto, (1999).
2. G.A. Greene, T. Ginsberg, and M.S. Kazimi, "Assessment of the Thermal Hydraulic Technology of the Transition Phase of a Core-Disruptive Accident in a LMFBR" , NUREG/CR-3014, Nov. (1982).
3. Alan E. Waltar and Albert B. Reynolds, "Fast Breeder Reactors", Pergamon Press, New York, Oxford, Toronto, Sydney, Paris, Frankfurt, pp. 609 - 610, (1980).
4. E.E. Lewis, "Nuclear Power Reactor Safety", A Wiley-interscience Public, New York, pp. 281 - 282, (1977).
5. F.E. Dunn, et al., "The SAS2A LMFBR Accident-Analysis Computer Code," ANL-8183, Oct. (1974).
6. Y.M. Kwon, et al., "Development of a System Analysis Code, SSC-K, for Inherent Safety Evaluation of the Korea Advanced Liquid Metal Reactor," J. Korean Nucl. Soc., vol.33, p.209-224, (2001).
7. M. Green, "FRAX, A Whole Core Accident Code for Fast Reactors", AEA, Presentations to KAERI, March (1998).
8. D.J. Brear, J.A. Moran, T. Rudge, "Fuel Pin loading and pin failure criteria in the UK code FRAX-5 under WCA condition", Fast Reactor Core and Fuel Structure Behavior, BNES, London, (1990).
9. T. Rudge, "Homsep-2 : A One-dimensional Sodium Boiling Model for the Fast Reactor", Nucl. Energy, 28, N0. 3, June, pp. 171-181, (1989).